catalysts

MDPI

Article

Pyridyl-Anchored Type BODIPY Sensitizer-TiO_2 Photocatalyst for Enhanced Visible Light-Driven Photocatalytic Hydrogen Production

Xiao-Feng Shen [1], Motonori Watanabe [1,2,3,*], Atsushi Takagaki [2,3], Jun Tae Song [2,3] and Tatsumi Ishihara [1,2,3]

1 Department of Automotive Science, Graduate School of Integrated Frontier Sciences, Kyushu University, 744 Motooka, Nishi-ku, Fukuoka 819-0395, Japan; shen.xiaofeng.524@s.kyushu-u.ac.jp (X.-F.S.); ishihara@cstf.kyushu-u.ac.jp (T.I.)
2 International Institute for Carbon-Neutral Energy Research (WPI-I2CNER), Kyushu University, 744 Motooka, Nishi-ku, Fukuoka 819-0395, Japan; atakagak@cstf.kyushu-u.ac.jp (A.T.); song.juntae@cstf.kyushu-u.ac.jp (J.T.S.)
3 Department of Applied Chemistry, Kyushu University, 744 Motooka, Nishi-ku, Fukuoka 819-0395, Japan
* Correspondence: mwata@i2cner.kyushu-u.ac.jp; Tel.: +81-92-802-6748

Received: 8 April 2020; Accepted: 8 May 2020; Published: 12 May 2020



Abstract: Dye-sensitized photocatalytic hydrogen production using a boron-dipyrromethene (BODIPY) organic material having a pyridyl group at the anchor site was investigated. Phenyl, carbazole, and phenothiazine derivatives were introduced into BODIPY dyes, and their photocatalytic activities were examined. Identification was performed by nuclear magnetic resonance (NMR), infrared (IR), mass (MS) spectra, and absorption spectra, and catalyst evaluation was performed by using visible-light irradiation and photocatalytic hydrogen production and photocurrent. These dyes have strong absorption at 600–700 nm, suggesting that they are promising as photosensitizers. When the photocatalytic activity was examined, stable catalytic performance was demonstrated, and the activity of the Pt-TiO_2 photocatalyst carrying a dye having a carbazole group was 249 μmol/g_{cat}·h. Photocurrent measurements suggest that dye-sensitized photocatalytic activity is occurring. This result suggests that BODIPY organic materials with pyridyl groups as anchor sites are useful as novel dye-sensitized photocatalysts.

Keywords: hydrogen; dye-sensitized; photocatalyst; photocurrent

1. Introduction

Research on new energy carriers that can replace fossil fuels is attracting attention. As a candidate, hydrogen can be compressed, stored, and transported, and it has a sufficient carrier density [1]. A hydrogen fuel cell is a CO_2-free system that only discharges water when extracting electricity. On the other hand, in the fossil fuel combustion method and methane steam reforming method, which are the mainstays of the current hydrogen production methods, the use of a carbon material source as a hydrogen source becomes a problem, and the production process produces carbon dioxide [2]. From this perspective, attention has been paid to hydrogen production by water splitting, using a hydrogen generation that is not derived from carbon source [3]. Photocatalytic water splitting is attracting attention as the most ideal hydrogen production method among water-splitting reactions [4]. In order to obtain high photocatalytic performance, research has been conducted on the construction of a high photo-electron conversion system with a small band gap, improvement of the reaction active site by changing the shape of the catalyst, and improvement of the efficiency of the water-splitting reaction by extending the life of charge separation [5]. On the other hand, research by half-reaction

of only hydrogen/oxygen sites is also important research for improving each reaction activity [6]. Among such research, there is a visible-light-responsive photocatalyst, using visible light, which is a component of 50% of sunlight. However, there are not many reports of highly efficient and stable visible-light-responsive photocatalysts [7]. Dye-sensitized photocatalysts can support various dye sensitizers on a stable photocatalyst and promise to develop a stable photocatalyst system, using the desired visible light [8]. Porphyrin is one of the dyes having a strong molar extinction coefficient in the visible-light region, and many studies have been reported [9]. However, this dye has a strong Soret band at 400–500 nm, and it is desired to develop a dye that can use the longer wavelength side. One such dye is boron-dipyrromethene (BODIPY), which has half the structure of porphyrins. It is known that BODIPY has an absorption band with a strong molar extinction coefficient at 500–900 nm [10] and has an electrochemically stable structure, and a new method for synthesizing BODIPY [11] and its related compounds [12], semiconductors and OPV [13], and biotechnology [14]. In recent years, BODIPY has attracted attention as a skeleton of photocatalysts. For hydrogen production, there have been reports on the introduction of molecular catalysts [15–17] and MOFs [18,19] into partial skeletons, dye-sensitized oxidation [20], CO_2 reduction [21], and other photocatalytic reactions [22–27]. Kubo et al. have developed a donor-acceptor dye by using π-extended BODIPY as the photo-donor site and have developed it into a dye-sensitized TiO_2 photocatalyst to achieve efficient photocatalytic hydrogen production [28]. An efficient photosensitization path by introducing a donor–acceptor structure into BODIPY enables the introduction of chromophores at the α, β, and meso positions [10,13]. At this time, an electron donor site can be introduced at the α and β positions, and an electron acceptor site can be introduced at the meso position [13]. The development of an efficient dye-sensitized solar cell using this strategy has been reported [29,30]. In this study, we developed a novel BODIPY dye with a pyridyl group at the α-position as an electron donor and an electron acceptor at the meso position (Figure 1). We have reported that these are titanium oxide photocatalysts and work as efficient and highly stable photosensitizers.

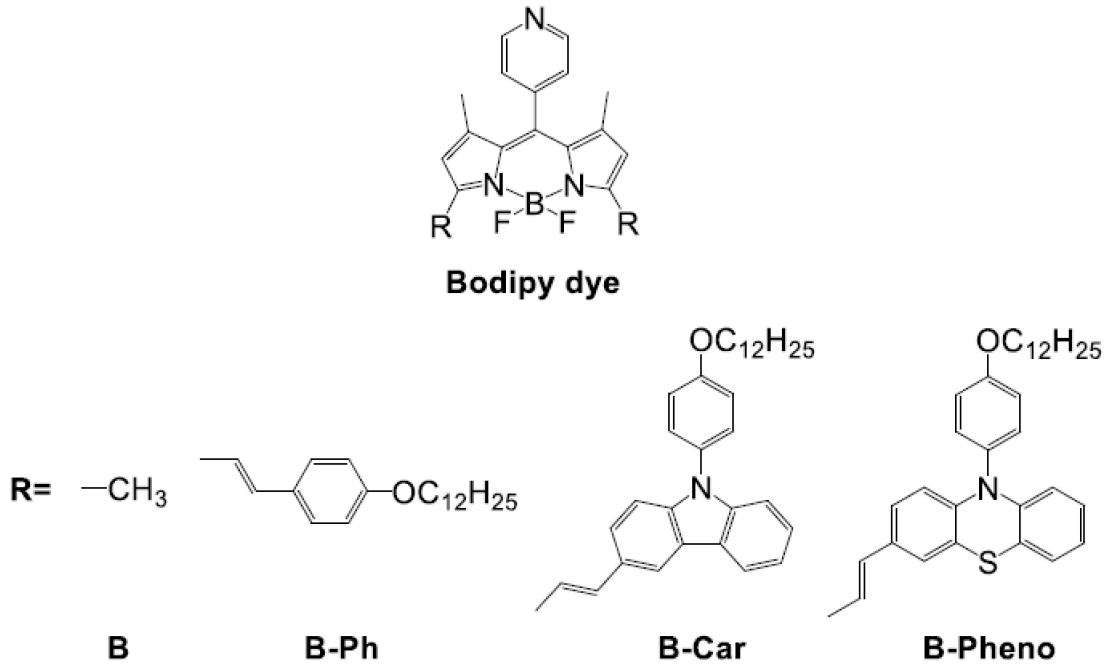
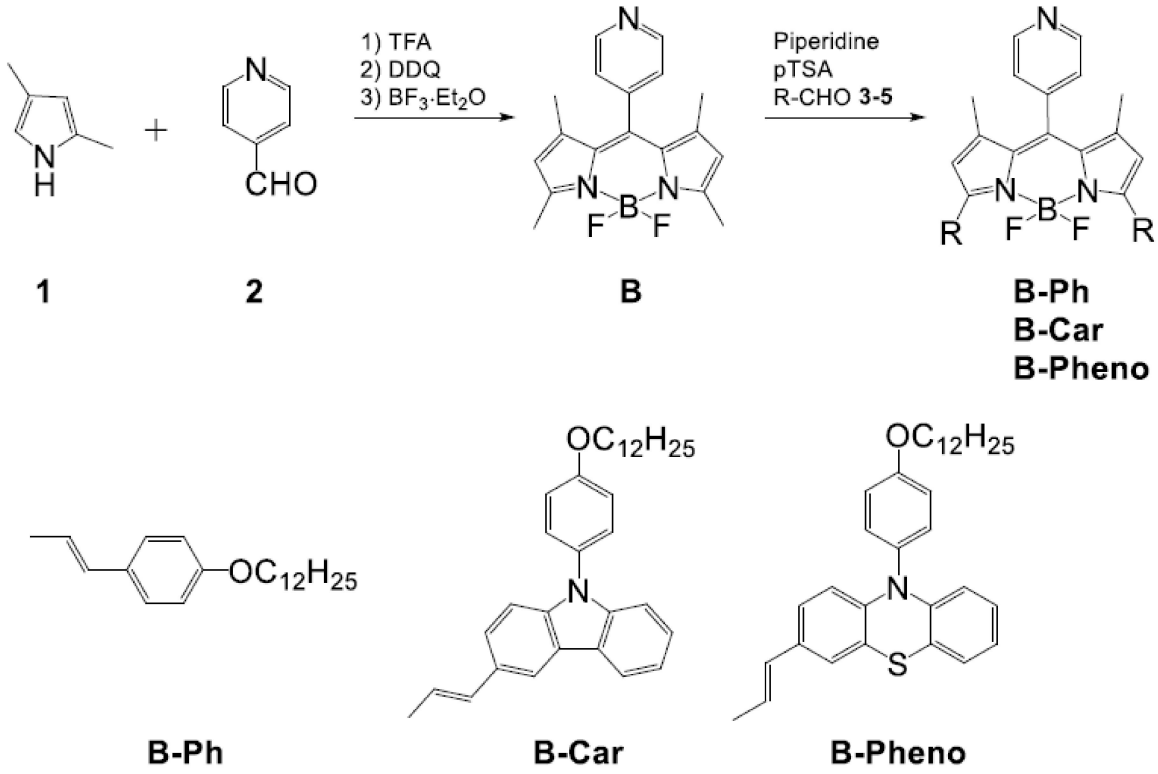


Figure 1. Chemical structure of BODIPY-sensitizer for this work.

2. Results and Discussion

2.1. Synthesis

Synthesis of BODIPY-sensitizers are illustrated in Scheme 1. Pyridine-boron-dipyrromethene pendants **B** was synthesized by reaction with 2,4-dimethyl-1H-pyrrole and isonicotinaldehyde in the catalytic amounts of trifluoroacetic acid (TFA), followed by oxidized with 2,3-dichloro-5,6-dicyano-p-benzoquinone (DDQ), and complexed with boron trifluoride–ethyl ether complex (BF_3-Et_2O) to obtain a yield of 16%. The π-conjugated system of the BODIPY core synthesized extended **B-Ph**, **B-Car**, and **B-Pheno** in 19%–53%, by reacting with aldehydes **3-5** in the presence of an acid catalyst. Since all dyes, **B**, **B-Ph**, **B-Car**, and **B-Pheno**, can be synthesized in four steps, dyes that can absorb visible light can be synthesized efficiently. Further details of the synthetic procedure are explained in the Supplementary Materials.



Scheme 1. Synthetic route of BODIPY-sensitizers. **3**: 4-(dodecyloxy)benzaldehyde, **4**: 9-(4-(dodecyloxy) phenyl)-9H-carbazole-3-carbaldehyde, **5**: 10-(4-(dodecyloxy)phenyl)-10H-phenothiazine-3-carbaldehyde.

2.2. Physical/Theoretical Properties of BODIPY Dyes B, B-Ph, B-Car, and B-Pheno

Absorption spectra of synthesized BODIPY **B**, **B-Ph**, **B-Car**, and **B-Pheno** were measured in THF solutions (Figure 2a). The lowest absorption peak of **B** shows at 503 nm with high molar extinction coefficient (ε = 52300). On the other hand, π-expanded BODIPY system **B-Ph**, **B-Car**, and **B-Pheno** show bathochromic shift and a change in molar express factor, **B-Ph** was 650 nm (ε = 141000), **B-Car** was 676 nm (ε = 36000), and **B-Pheno** was 699 nm (ε = 21000). Among the π-extended molecules, the phenyl group-introduced molecule had the smallest bathochromic shift but a high molar extinction coefficient, while the phenothiazine-group-introduced molecule had a large bathochromic shift but a small molar extinction coefficient. The highest occupied molecular orbitals (HOMOs) and lowest occupied molecular orbitals (LUMOs) for **B**, **B-Ph**, **B-Car**, and **B-Pheno** are estimated by cyclic- and pulse- voltammetry in 0.1 M nBu_4NPF_6 THF solution (Figure 2b). The oxidation and reduction peaks showed at +1.37 V (vs. NHE) and −0.99 V (vs. NHE) for **B**; +0.99 V (vs. NHE) and −0.79 V (vs. NHE)

for **B-Ph**; +0.89 V (vs. NHE) and −0.81 V (vs. NHE) for **B-Car**; and +0.87 V (vs. NHE) and −0.77 V (vs. NHE) for **B-Pheno**, respectively. All HOMO-LUMO gaps of **B-Ph**, **B-Car**, and **B-Pheno** (1.64–1.78 V vs. NHE) were reduced compared to **B** (2.36 V vs. NHE). This suggests that the oxidation potential of aromatics containing **B-Ph**, **B-Car**, and **B-Pheno** increased, and the reduction potential decreased compared to **B**.

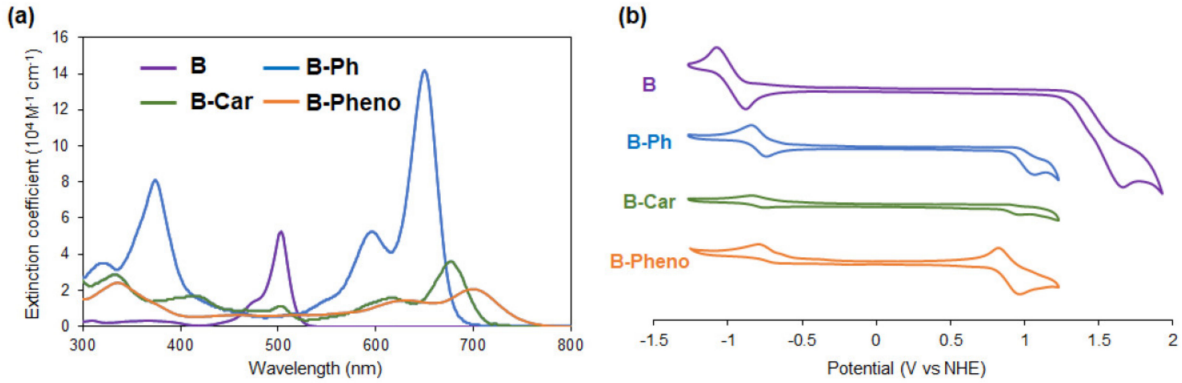


Figure 2. (**a**) Absorption and (**b**) CV spectra of **B**, **B-Ph**, **B-Car**, and **B-Pheno** in THF solution.

Figure 3 (left) shows the DFT computation results of **B**, **B-Ph**, **B-Car**, and **B-Pheno**. The dihedral angle between the BODIPY core and the pyridyl group of **B** is 90 degrees, which means that the conjugation between these two parts is very weak. In **B-Ph**, **B-Car**, and **B-Pheno**, the dihedral angle between the BODIPY core and the pyridyl group are 89.5–90 degrees, as in **B**. On the other hand, the dihedral angle between the BODIPY core and the π-conjugated aromatic component is 3.9 degrees for **B-Ph**, 9.4 degrees for **B-Car**, and 7.9 degrees for **B-Pheno**. Thus, the dihedral angle between BODIPY and aromatic at **B-Ph**, **B-Car**, and **B-Pheno** is very small, and an efficient π-conjugate interaction is expected. Figure 3 (right) shows HOMO and LUMO orbitals of **B, B-Ph**, **B-Car**, and **B-Pheno**. BODIPY **B** of HOMO and LUMO are delocalized on dipyrrolomethane moiety, while no HOMO and LUMO orbitals on pyridyl group due to weak conjugation between BODIPY and pyridyl groups. In **B-Ph**, **B-Car**, and **B-Pheno**, HOMO and LUMO orbitals were delocalized to the extended aromatic moieties in addition to the BODIPY core, supporting the absorption spectra of bathochromic shifts and electrochemical measurements of lower HOMO-LUMO gaps. From the overlap of HOMO and LUMO on the BODIPY and aromatic core in **B, B-Ph**, **B-Car**, and **B-Pheno**, assigned to the π–π* transition type interaction. **B**, **B-Ph**, **B-Car**, and **B-Pheno** were loaded to the catalyst by suspending 0.75wt% Pt-TiO_2 in THF solutions of the dyes. Figure 4 illustrates the reflectance spectra of **B, B-Ph**, **B-Car**, and **B-Pheno**/Pt-TiO_2. The loading amounts of the sensitizers on the catalysts were subsequently assessed. The amount of loaded dye was estimated based on the remaining amount of the THF solution, which was separated from the photocatalyst by centrifugation. Accordingly, the loading of the dye in the **B**/Pt-TiO_2 system was determined at 17.8 μmol/g, while in **B-Ph**/Pt-TiO_2, it was 10.0 μmol/g. Moreover, the sensitizer loading in **B-Car**/Pt-TiO_2 was established at 7.5 μmol/g, whereas, in the **B-Pheno**/Pt-TiO_2 system, it was estimated at 6.8 μmol/g. These values are consistent with the dye-loading amounts previously reported for a porphyrin–pyridine pendant system [31]. Notably, the loading amount of dye **B** on the catalyst was the largest. This is because **B-Ph**, **B-Car**, and **B-Pheno** contain bulky alkyl groups, leading to alkyl chain packing on TiO_2. The lowest energy peaks for **B**, **B-Ph**, **B-Car**, and **B-Pheno** on Pt-TiO_2 appeared at 516, 689, 709, and 692 nm, respectively. The **B**, **B-Ph**, and **B-Car** dyes exhibited a peak broadening and a red shift. The adsorption modes of all the dyes and TiO_2 are considered to be the same Lewis acid interaction (discussed later), suggesting that there are no differences in the adsorption modes. It is speculated that the reason for the peak shift is the formation of J-aggregates on titanium oxide by the **B**, **B-Ph**, and **B-Car** dyes. On the other hand, owing to the presence of a more flexible phenothiazine moiety, which is involved in a weak electronic interaction

between the **B-Pheno** dye and titanium oxide, no significant change in the absorption spectrum was observed for **B-Pheno**/Pt-TiO_2.

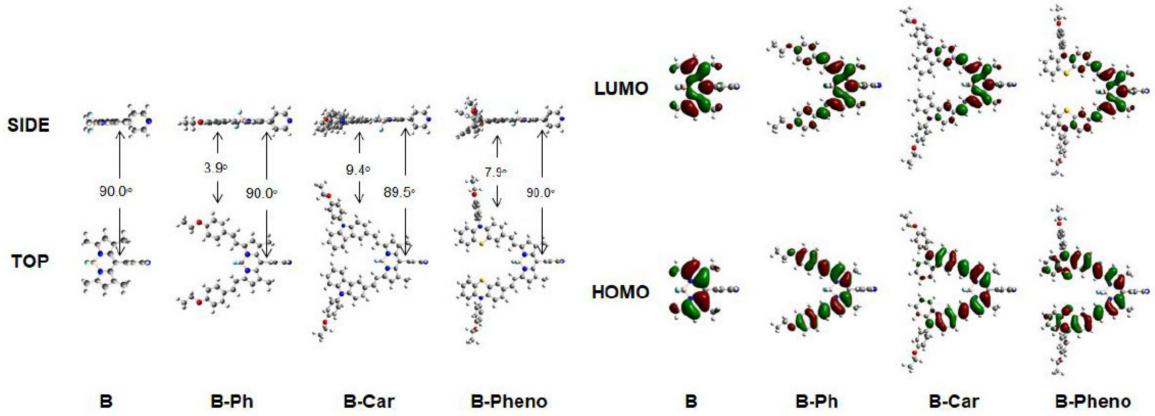


Figure 3. (**Left**) Optimized structure at B3LYP/6-31G(g) level and dihedral angles of **B**, **B-Ph**, **B-Car**, and **B-Pheno**. (**Right**) HOMO and LUMO orbitals of **B**, **B-Ph**, **B-Car**, and **B-Pheno**.

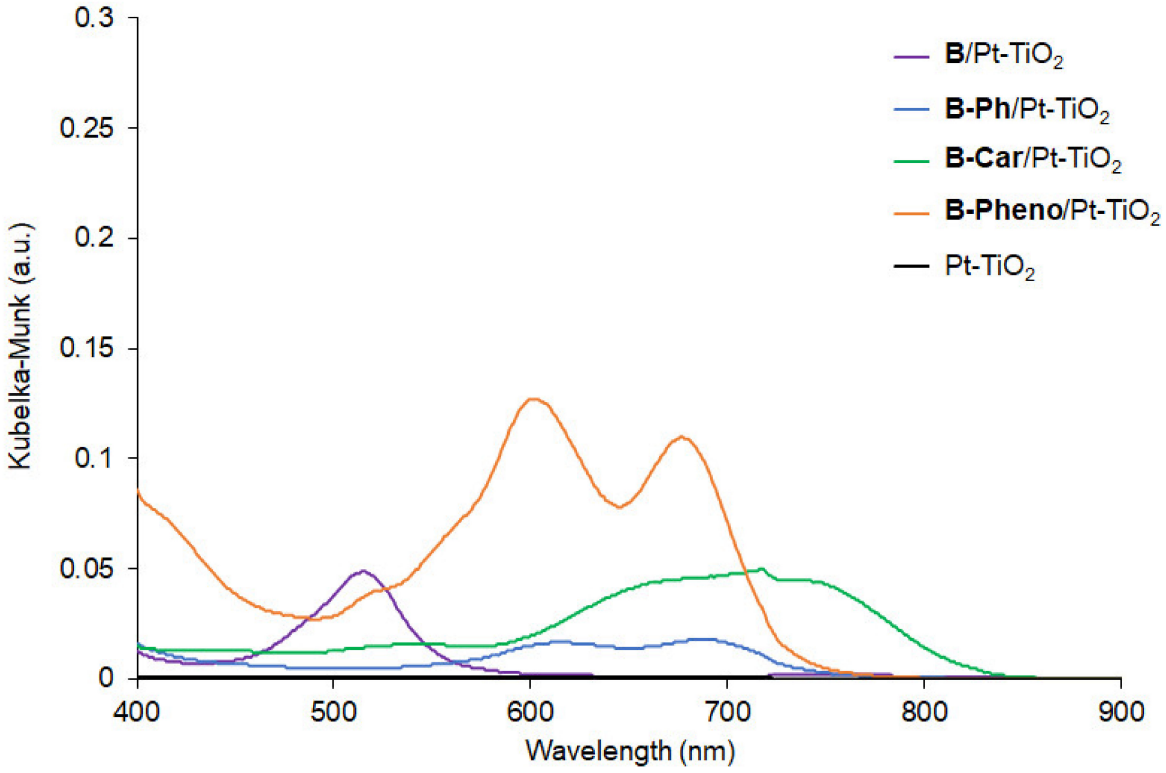


Figure 4. Reflectance spectra of **B, B-Ph**, **B-Car**, and **B-Pheno**/Pt-TiO_2.

To confirm the adsorption of the dyes on TiO_2, we measured the IR absorption spectra (Figure 5). The bulk powders of the **B**, **B-Ph**, **B-Car**, and **B-Pheno** dyes were analyzed, and vibration modes corresponding to the pyridyl moiety appeared at 1600 cm^{-1} for **B**, 1608 cm^{-1} for **B-Ph**, 1612 cm^{-1} for **B-Car**, and 1596 cm^{-1} for **B-Pheno**. Pt-TiO_2 exhibited an absorption at 1647 cm^{-1}, which belonged to the vibration mode of adsorbed water. For **B**, **B-Ph**, **B-Car**, and **B-Pheno**/Pt-TiO_2, the peak at 1647cm^{-1} shifted, and the appearance of peaks at 1631 and 1442 cm^{-1} (**B**/Pt-TiO_2), 1635 and 1438 cm^{-1} (**B-Ph**/Pt-TiO_2), 1631 and 1434 cm^{-1} (**B-Car**/Pt-TiO_2), and at 1635 and 1446 cm^{-1} (**B-Pheno**/Pt-TiO_2) was observed. When the pyridyl anchor moiety was changed to a phenyl group, the Pt-TiO_2 loading test demonstrated that compound **B-ref** did not show this characteristic peak in the reflectance spectra

(Supplementary Figure S1a,b). However, a peak at 1542 cm^{-1} was observed in the IR spectrum of the **B-ref**. Following the Pt-TiO_2 loading test, the peak at 1644 nm^{-1} did not shift, indicating that the dye was not adsorbed on the TiO_2 surface in the absence of a pyridyl moiety (Supplementary Figure S1c). The pyridyl group is known as an anchor site to titanium oxide [32]. The observed peaks were attributed to adsorption involving a Lewis-acid-type coordination bond to titanium oxide [33]. This implies that the pyridyl moiety is adsorbed on the titanium oxide surface via a N-Ti coordinate-type bond between the nitrogen atom of the pyridyl group and metal in the TiO_2. The physical and theoretical properties of the BODIPY dyes, i.e., **B, B-Ph**, **B-Car**, and **B-Pheno**, are summarized in Table 1.

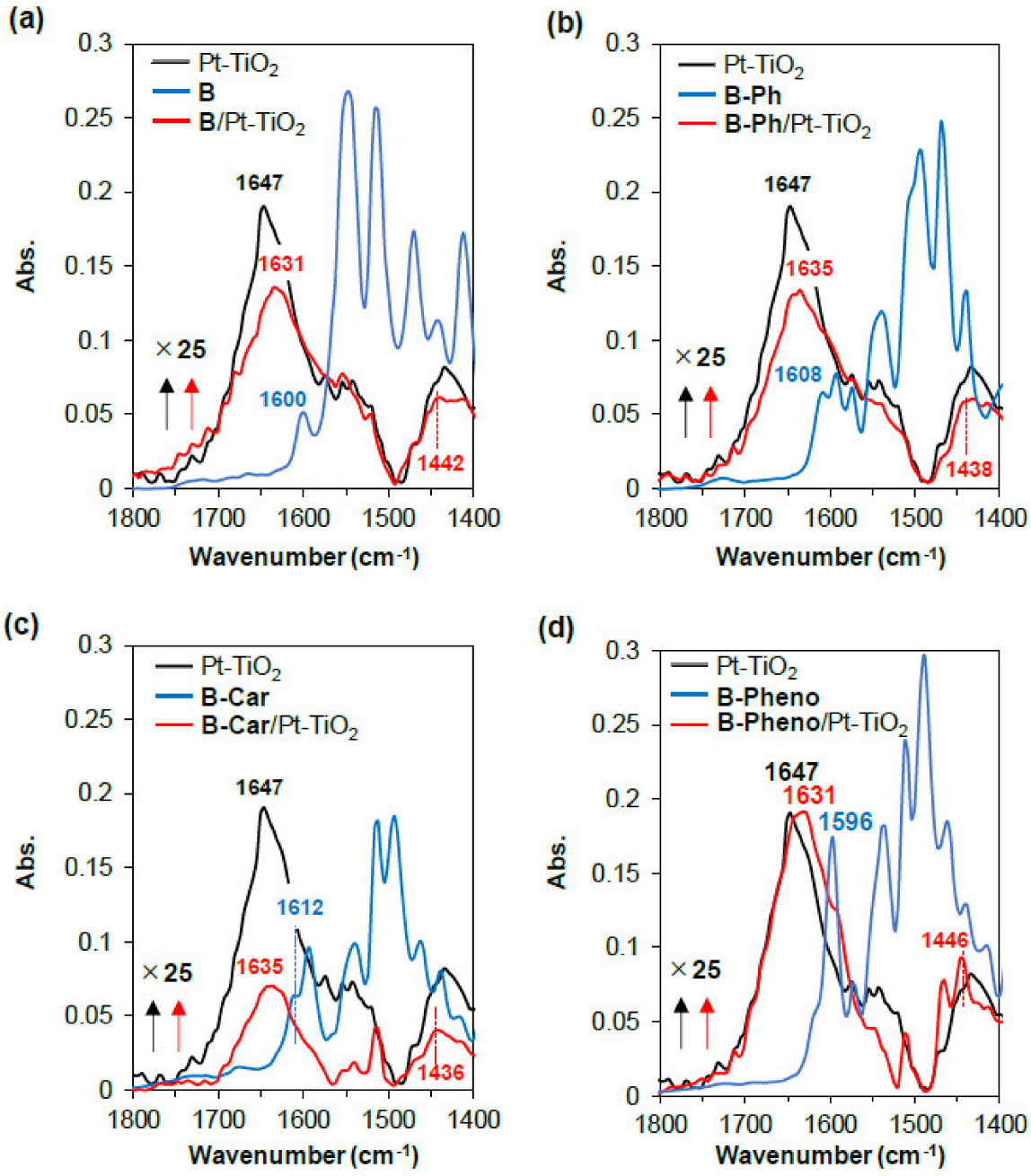


Figure 5. IR spectra of (**a**) **B** and **B/**Pt-TiO_2; (**b**) **B-Ph** and **B-Ph/**Pt-TiO_2; (**c**) **B-Car** and **B-Car/**Pt-TiO_2; and (**d**) **B-Pheno** and **B-Pheno/**Pt-TiO_2.

Table 1. Physical/theoretical properties of **B, B-Ph**, **B-Car**, and **B-Pheno**.

Sample	Abs. at soln. [a] (nm/ε)	Abs. on Pt-TiO_2 [b] (nm)	Oxidation Potential [a] (V vs NHE)	Reduction Potential [a] (V vs NHE)	Energy Gap [d] (V vs NHE)	HOMOv [e] (eV)	LUMOv [e] (eV)	Energy Gapv [e] (eV)
B	503/5,2300	516	- [c] +1.37 [d]	−0.98 [c] −0.99 [d]	2.36	−5.51	−2.53	2.99
B-Ph	650/14,1000	689	- [c] +0.99 [d]	−0.78 [c] −0.79 [d]	1.78	−4.69	−2.55	2.14
B-Car	676/3,6000	709	+0.94 [c] +0.89 [d]	−0.76 [c] −0.81 [d]	1.70	−4.51	−2.43	2.08
B-Pheno	699/2,1000	692	+0.85 [c] +0.87 [d]	- [c] −0.77 [d]	1.64	−4.47	−2.49	1.98

a: in THF; b: **dye**/0.75wt%Pt-TiO_2/FTO; c: cyclic voltammetry and d: difference pulse voltammetry was measured in 0.1M nBu_4MPF_6 THF solution. The potentials were calibrated according to Fc/Fc^+ = −0.63 V vs. NHE.; e: estimated by B3LYP/6-31G(d) level.

2.3. Photocatalytic Reaction

The visible-light-driven photocatalytic hydrogen production in water medium using **B, B-Ph**, **B-Car**, and **B-Pheno**/0.75wt%Pt-TiO_2 nanoparticles was investigated. The dye-loaded 0.75 wt% Pt-TiO_2 catalyst powder was suspended in water, with ascorbic acid (pH 4) acting as a sacrificial reagent. This suspension was purged with argon, and a Xe lamp (>420 nm filter) was used to irradiate the system. Further, the amount of hydrogen gas output was measured by using the thermal conductivity detector-gas chromatography (Figure 6a). When the hydrogen production reaction of **B, B-Ph**, **B-Car**, and **B-Pheno**/0.75wt%Pt-TiO_2 were tested in dark condition, no hydrogen production was confirmed (Supplementary Figure S2). In this experiment, 0.75wt% Pt-TiO_2, which does not carry a dye, hardly generated hydrogen (8.0 μmol/g_{cat}·h) because it cut off ultraviolet light (>420 nm). On the other hand, in the case of dye **B, B-Ph**, **B-Car**, and **B-Pheno**/0.75wt% Pt-TiO_2, the generation of hydrogen under visible-light irradiation increased. These results suggest that the dye acted as a sensitizer under visible-light irradiation and improved the photocatalytic ability. The hydrogen production rates were in the order of **B-Car**/0.75wt% Pt-TiO_2 (249 μmol/g_{cat}·h) > **B-Pheno**/0.75wt% Pt-TiO_2 (235 μmol/g_{cat}·h) > **B**/0.75wt% Pt-TiO_2 (187 μmol/g_{cat}·h) > **B-Ph**/0.75wt% Pt-TiO_2 (97 μmol/g_{cat}·h). Figure 6b demonstrates the hydrogen production efficiency as a turnover number (TON), which was used to evaluate the catalytic reactivity of dye-sensitizer **B**, **B-Ph**, **B-Car**, and **B-Pheno**. In addition, the turnover frequency (TOF) values of the dye-loaded catalysts were in the following order: **B-Car**/0.75wt% Pt-TiO_2 (63.2 μmol/g_{cat}·h) ≈ **B-Pheno**/0.75wt% Pt-TiO_2 (63.1 μmol/h) > **B**/0.75wt% Pt-TiO_2 (21.7 μmol/h) > **B-Ph**/0.75wt% Pt-TiO_2 (19.7 μmol/h). Following the photocatalytic hydrogen production, the suspended photocatalyst solutions were separated to the aqueous solutions and catalysts by centrifugation. Soluble substances in the aqueous solution were extracted with $CHCl_3$. The absorption spectra of **B**, **B-Ph**, **B-Car**, and **B-Pheno** in $CHCl_3$ did not show any absorption peaks, suggesting that the dyes did not desorb in the solutions during the photoreaction (Supplementary Figure S3a). Moreover, following the photocatalytic reaction in the presence of the catalysts **B**/Pt-TiO_2 and **B-Ph**/Pt-TiO_2 showed broad peaks, while no noteworthy changes were observed for **B-Car**/Pt-TiO_2 and **B-Pheno**/Pt-TiO_2 (Supplementary Figure S3b). We considered that the differences in the orientations of **B-Car**/Pt-TiO_2 and **B-Pheno**/Pt-TiO_2 before and after the reaction were small, because both **B-Car** and **B-Pheno** exhibit bulkier structures, enabling the formation of optimal packing structures on titanium oxide [34]. To further confirm the stability of the photocatalyst, we conducted a **B-Car**/Pt-TiO_2 recycle test (Figure 7). The photocatalytic reaction involving **B-Car**/Pt-TiO_2 was repeated five times. After five sequences lasting 24 h each (120 h in total), the dye remained active, suggesting that the catalyst was stable and reusable.

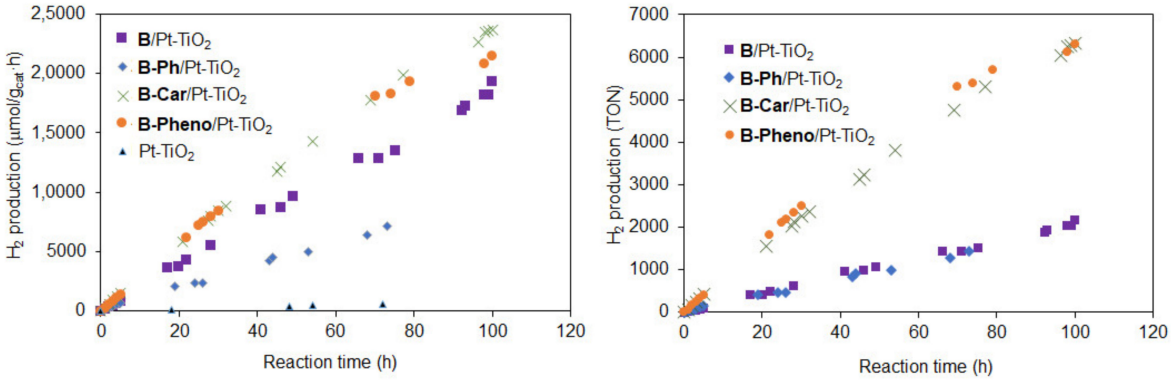


Figure 6. Photocatalytic hydrogen production results of **B, B-Ph**, **B-Car**, and **B-Pheno**/Pt-TiO_2 in water medium. (**Left**) Hydrogen production rate vs reaction time plot. (**Right**) Turn over number of hydrogen production from dye-sensitizer **B, B-Ph**, **B-Car**, and **B-Pheno** vs. reaction time plot. Conditions: Xe lamp (0.15 mW/cm^2 after filtered with long path filter of > 420 nm), 0.57 M ascorbic acid aq. (pH = 4.0).

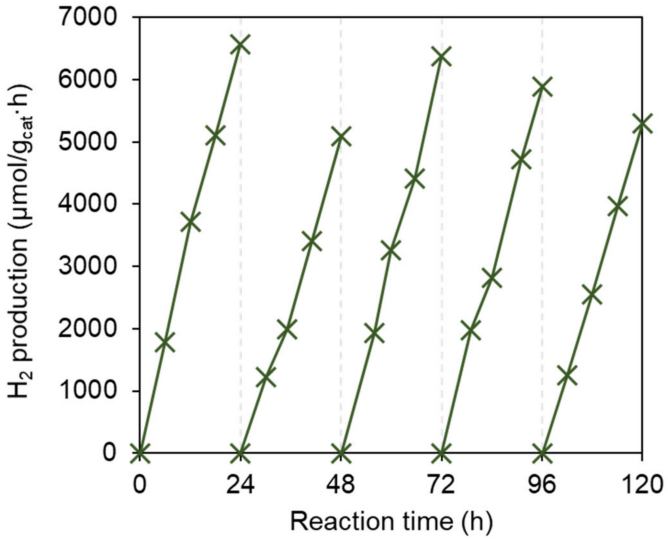


Figure 7. Recycle test showing hydrogen production results for **B-Car**/Pt-TiO_2. Conditions: Xe lamp (0.15 mW/cm^2), 0.57 M ascorbic acid aq. (pH = 4.0).

To elucidate the hydrogen production mechanism, the photocatalytic reaction of **B-Car**/TiO_2 with and without a UV cut filter (>420 nm) was investigated. No hydrogen was detected under dark conditions (Supplementary Figure S2). On the other hand, the production of hydrogen was evident under visible light conditions (Figure 6 and Supplementary Figure S4). It is noteworthy that the photocatalytic reaction without a >420 nm filter enhanced the photocatalytic activity. This outcome implied that the developed photocatalyst was effective in the visible-light-driven photocatalytic reactions. Conversely, the photocatalytic reaction with **B-Car**/TiO_2 in the absence of Pt did not produce hydrogen under visible light, demonstrating the critical role of the Pt cocatalyst in this photocatalytic system (Supplementary Figure S4).

To further evaluate the visible light-driven photo-induced catalytic reactions involving the sensitizers, fluorescence decay spectra of **B**, **B-Ph**, **B-Car**, and **B-Pheno** were measured. Figure 8a illustrates the fluorescence decay spectra of **B**, **B-Ph**, **B-Car**, and **B-Pheno** in THF, whereas Figure 8b shows the spectra of **B**, **B-Ph**, **B-Car**, and **B-Pheno** on 0.75wt% Pt-TiO_2. The decay lifetimes for the THF solutions were in the following order: **B-Car** (τ = 24.06 ns) > **B-Ph** (τ = 19.80 ns) > **B-Pheno** (τ = 19.48 ns) > **B** (τ = 15.93 ns). Moreover, for the catalysts, the decay lifetimes were in the order of **B-Car** (τ = 4.85 ns) > **B-Pheno** (τ = 4.56 ns) > **B-Ph** (τ = 3.13 ns) > **B** (τ = 2.77 ns). The fluorescence

lifetime was shorter for the samples, in which the dyes were adsorbed on Pt-TiO_2 than for samples of the sensitizers in the THF. The fluorescence spectra of **B**, **B-Ph**, **B-Car**, and **B-Pheno** displayed peaks over 500 nm (Supplementary Figure S5, in THF). This implies that the fluorescence and absorption spectra of TiO_2 cannot overlap; thus, the occurrence of energy transfer can be ruled out. Overall, our observations suggest an efficient electron transfer from the dye to Pt-TiO_2 under visible-light irradiation.

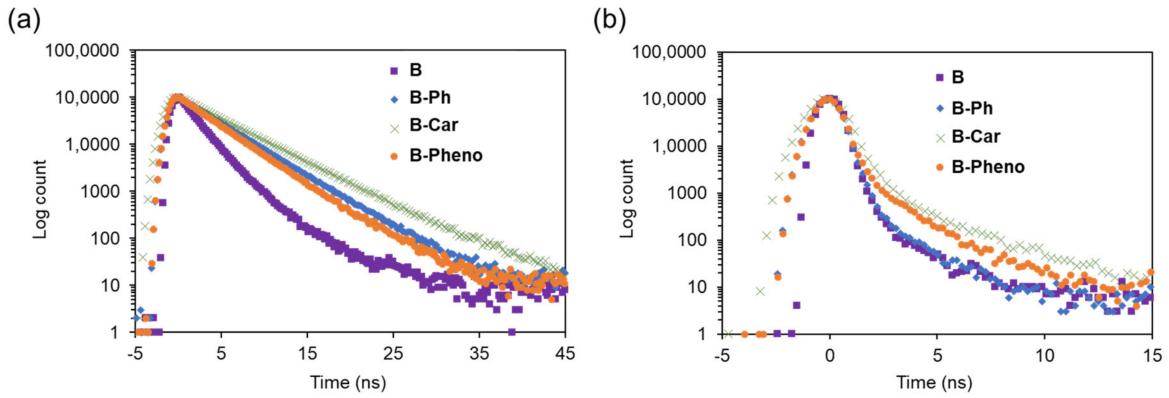


Figure 8. Fluorescence decay spectra of (**a**) **B, B-Ph**, **B-Car**, and **B-Pheno** in THF solution and (**b**) **B, B-Ph**, **B-Car**, and **B-Pheno** on 0.75wt% Pt-TiO_2.

Figure 9 shows photocurrent spectra of **B, B-Ph**, **B-Car**, and **B-Pheno**/0.75wt% Pt-TiO_2 film under visible-light (> 420 nm) irradiation. Under chopped illumination, the photocurrent of intensity order showed **B-Car**/Pt-TiO_2 > **B-Pheno**/Pt-TiO_2 > **B**/Pt-TiO_2 > **B-Ph**/Pt-TiO_2 > Pt-TiO_2. The higher photocurrent suggested increasing of the electron carrier concentration into TiO_2 of conduction band [35]. However, all dyes showed an unstable character after the photocurrent spike; the decreasing of the photocurrent rapidly under photo illumination indicated that a fast charge-recombination process occurred between dyes and TiO_2 surfaces [36]. The order of photocurrent follows the same tendency as the hydrogen production rate or TOF, as the suggested number of excited photons played a critical role in the production of hydrogen in the **B**-, **B-Ph**-, **B-Car**-, and **B-Pheno**-loaded photocatalyst system. As a result of DFT calculation, the orbits of all the dyes were delocalized in the BODIPY skeleton for both HOMO–LUMO, and the pyridyl group as the anchor site did not have orbitals. From the result of IR spectrum, the dye was adsorbed on titanium oxide via the pyridyl group. Furthermore, the fluorescence lifetime spectrum suggested that electron transfer occurred from the dyes to titanium oxide. The fact that all dyes produce higher photocurrents than titanium oxide alone indicates that efficient through-space-type charge transfer from the sensitizer to titanium oxide occurs under visible light, resulting in hydrogen production.

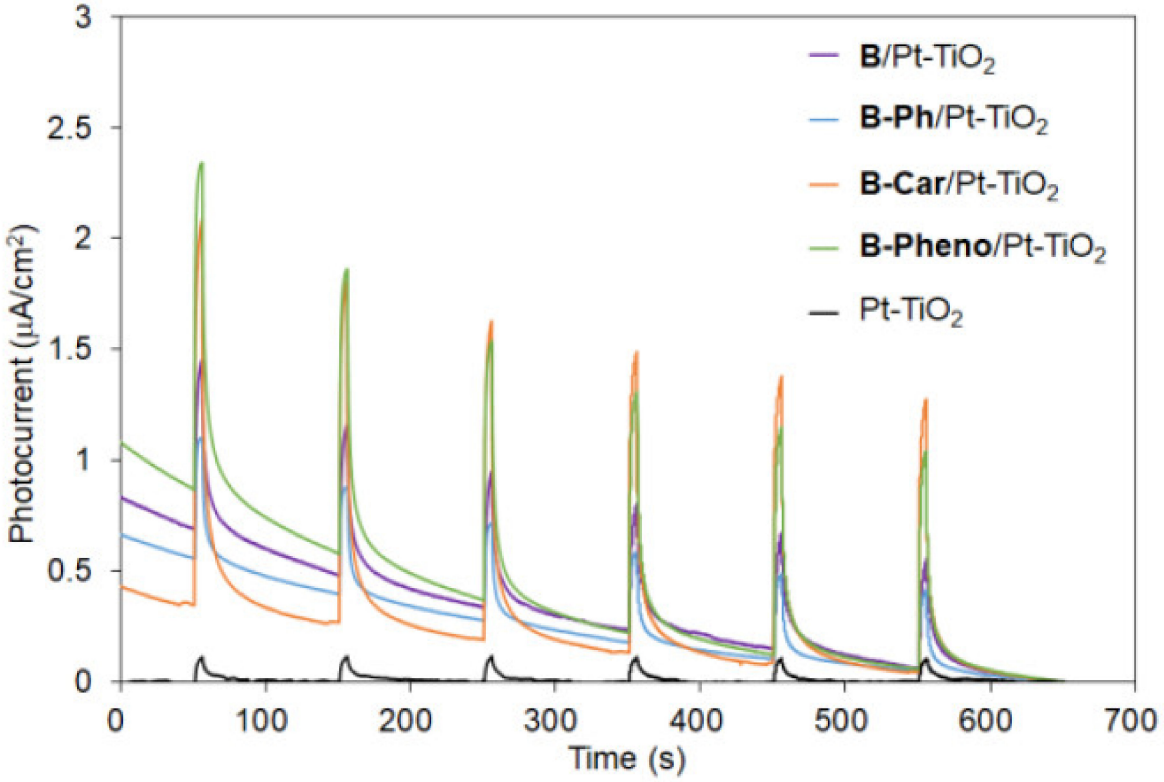


Figure 9. Photocurrent spectra of **B, B-Ph**, **B-Car**, and **B-Pheno**/0.75wt% Pt-TiO_2 film under visible light (filtered with long path filter of > 420 nm).

The results of photocatalytic hydrogen production and photocurrent irradiation in water under visible-light irradiation suggest that electrons are injected from the dye into the Pt-TiO_2 catalyst in the excited state of dyes **B, B-Ph**, **B-Car**, and **B-Pheno**, and that a catalytic reaction occurs. Figure 10a summarizes the energy diagram of **B, B-Ph**, **B-Car**, and **B-Pheno,** 0.75wt% Pt-TiO_2, and ascorbic acid, while Figure 10b illustrated the proposed reaction mechanism of photocatalytic reaction. Under visible-light (>420 nm) irradiation, **B, B-Ph**, **B-Car**, and **B-Pheno** of HOMO (+1.37 to +0.87 V vs. NHE) electrons are excited to LUMO (−0.99 to −0.77 V vs. NHE), and excited-state dyes **B, B-Ph**, **B-Car**, and **B-Pheno** were generated. The LUMO potential is more negative than TiO_2 CB (−0.50 V vs. NHE) and provides sufficient driving force for electron injection from excited state **B, B-Ph**, **B-Car**, and **B-Pheno** into the conduction band of TiO_2. The injected electrons move to the cocatalyst of platinum (Pt) and react with protons (H^+) to generate hydrogen. In this reaction, the BODIPY dye becomes an oxidized dye after injecting electrons into titanium oxide in the excited state. As an electron donor, ascorbic acid (AA) (Figure 10b, + 0.46 V vs. NHE) transfers electrons to the oxidized dyes and converted to dehydroascorbic acid (DHA) (Figure 10b) [37]. Correspondingly, oxidized dyes are reduced by accepting electrons from AA, affording BODIPY dyes, which exhibit catalytic activity. During a photocatalytic reaction, the photo-generated chemical species include the oxidized dye, hydrogen, and DHA. Thus, if the oxidized dyes react with the BODIPY dyes prior to receiving electrons from AA, the photocatalytic activity should be suppressed. Nonetheless, the recycle test shown in Figure 7 demonstrated that the hydrogen production rate does not change, and the catalyst retains its stability. The same photocatalytic activity was determined, meaning that the oxidized dye rapidly received electrons from AA and returned to the BODIPY form. To confirm the reactivity of these photo-generated species, we carried out a ^{1}H nuclear magnetic resonance (NMR) analysis of **B-Car** in the presence of hydrogen gas and the aqueous solution after the photoreaction (i.e., the DHA solution [37]). The obtained ^{1}H NMR results showed no changes in the conducted experiment (Supplementary Figure S6). Hence, the dye was determined to be stable to photogenerated

hydrogen and DHA. It was also confirmed that, as an electron donor, the oxidized dye transferred electrons to titanium oxide in the photoexcited state and reacted with AA, resulting in a stable catalytic cycle. This phenomenon leads to charge separation and photocatalytic hydrogen generation observed in the dye/Pt–TiO_2–AA system.

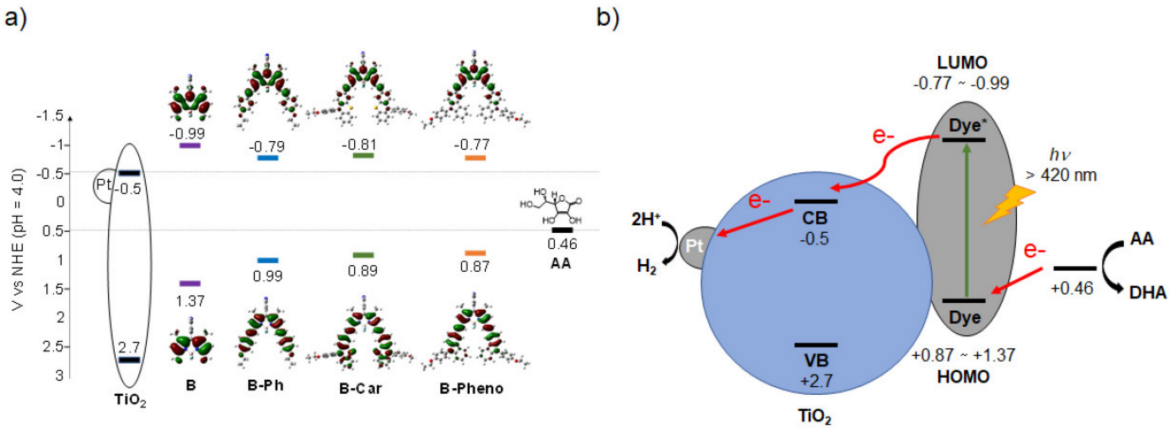


Figure 10. (**a**) Energy diagram of dyes (**B, B-Ph**, **B-Car**, and **B-Pheno**), 0.75wt% Pt-TiO_2, and ascorbic acid. (**b**) Proposed mechanism of the photocatalytic reaction.

3. Materials and Methods

TiO_2, (Sigma-Aldrich, Japan, anatase nanopowder, <25 nm particle size, 99.7% trace metals basis, surface area 45–55 m^2/g) and chloroplatinic acid hexahydrate (Sigma-Aldrich, Japan, 8 wt.% in H_2O) were used as the starting materials. Photodeposition in methanol was used to obtain 0.75wt% Pt-TiO_2. 0.75wt% Pt-TiO_2 (100 mg) was suspended in a THF solution of **B**, **B-Ph**, **B-Car**, and **B-Pheno** and allowed to stand at room temperature for 26 h, in the dark. The amount of loaded dye was estimated based on the remaining amount of the THF solution, which was separated from the photocatalyst by centrifugation. The photocatalytic hydrogen production reaction was performed by utilizing a quartz-closed reactor circulating system equipped with a thermal conductivity detector (Ar-carrier, column: molecular sieve 4Å, Shimadzu, Japan, GC-8A). The aqueous reaction solution contained the catalyst powder (20 mg), DI water, and 0.56 M AA as the sacrificial reagent (18 mL, pH 4 adjusted by NaOH). The photocatalytic reaction was performed by using a solar simulator (0.23 mW/cm^2, HAL-302, ASAHI spectra, Japan, 0.15 W/cm^2 after a >420 nm filter). The absorption/reflectance spectra were obtained by using a Shimadzu UV-3600 spectrophotometer. Cyclic voltammetry and photocurrent spectra were recorded on an electrochemical analyzer (ALS Co., Ltd, Japan, BAS ALS-1200C). IR spectra were tested by ATR-IR (Thermo Scientific, Japan, Nicolet iN10 MX). The fluorescence decay spectra were measured by employing a fluorescence lifetime spectrofluorometer (HORIBA, Japan, TemPro). The utilized excitation laser was 494 nm nanoLED for **B** and 631 nm nanoLED for **B**, **B-Ph**, **B-Car**, and **B-Pheno**. The DFT analysis was carried out by Gaussian 16 C 01. The synthetic details concerning the **B**, **B-Ph**, **B-Car**, and **B-Pheno** dyes are included in the Supplementary Materials.

4. Conclusions

In conclusion, new absorption was observed in the range from 400 to 700 nm by modifying **B, B-Ph**, **B-Car**, and **B-Pheno** to TiO_2. The lowest absorption peak of **B** shows at 503 nm with a high molar extinction coefficient (ε = 52300). On the other hand, π-expanded BODIPY system **B-Ph**, **B-Car**, and **B-Pheno** show bathochromic shift and a change in the molar extinction coefficient, **B-Ph** was 650 nm (ε = 141000), **B-Car** was 676 nm (ε = 36000), and **B-Pheno** was 699 nm (ε = 21000). From the results of CV and DFT, the dye HOMO-LUMO was localized in BODIPY and the extended aromatic compound, and the pyridyl group had no charge. This suggests that the light injection from the dye into the titanium oxide is a through-space-type injection. When conducting a photocatalytic reaction

with **B-Ph**, **B-Car**, and **B-Pheno**/0.75wt% Pt-TiO_2, more photocatalytic activity than 0.75wt% Pt-TiO_2 was confirmed in all modified organic dye **B-Ph**, **B-Car**, and **B-Pheno**. The hydrogen production rates of orders were **B-Car**/0.75wt% Pt-TiO_2 (249 μmol/g_{cat}·h) > **B-Pheno**/0.75wt% Pt-TiO_2 (235 μmol/g_{cat}·h) > **B**/0.75wt% Pt-TiO_2 (187 μmol/g_{cat}·h) > **B-Ph**/0.75wt% Pt-TiO_2 (97 μmol/g_{cat}·h). The photocurrent of intensity order showed **B-Car**/0.75wt% Pt-TiO_2 > **B-Pheno**/0.75wt% Pt-TiO_2 > **B**/0.75wt% Pt-TiO_2 > **B-Ph**/0.75wt% Pt-TiO_2 > 0.75wt% Pt-TiO_2. This order shows a similar tendency with hydrogen production rate, as the suggested number of excited photons played a critical role in the production of hydrogen in the **B-Ph-**, **B-Car-**, and **B-Pheno**-loaded photocatalyst system. When the photocatalytic activity was examined, stable catalytic performance was demonstrated, and the activity of the Pt-TiO_2 photocatalyst carrying a dye having a phenyl group was 400 μmol/h. Photocurrent measurements suggest that dye-sensitized photocatalytic activity is occurring. This result suggests that BODIPY organic materials with pyridyl groups as anchor sites are useful as novel dye-sensitized photocatalysts.

Supplementary Materials: The following data are available online at http://www.mdpi.com/2073-4344/10/5/535/s1. Figure S1: (a) Absorption spectra of B-ref in THF. (b) Diffuse reflectance spectra of B-ref before (red) and after (black) the Pt-TiO_2 loading test. (c) IR spectra of B-ref (blue) and B-ref before (red) and after (black) the Pt-TiO_2 loading test. Figure S2: Hydrogen production results for dye/Pt-TiO_2. Figure S3: (a) Absorption spectra of B, B-Ph, B-Car, and B-Pheno after the photocatalytic reaction in $CHCl_3$. (b) Diffuse reflectance spectra of Dye/Pt-TiO_2 before and after the photocatalytic reactions. Figure S4: Photocatalytic hydrogen production results for B-Car/Pt-TiO_2 (>420 nm filter, 0.15 mW/cm^2), B-Car/Pt-TiO_2 (irradiated without filter, 0.23 mW/cm^2), and B-Car/TiO_2 (>420 nm filter, 0.15 mW/cm^2). Figure S5: Diffuse reflectance spectra of Pt-TiO_2, and fluorescence spectra of B, B-Ph, B-Car, and B-Pheno in THF. Figure S6: ^{1}H NMR spectra for the reactivity test of B-Car with photogenerated species. Figure S7: ^{1}H NMR spectra of B (400 MHz). Figure S8: ^{13}C NMR spectra of B (100 MHz). Figure S9: ^{1}H NMR spectra of 3 (400 MHz). Figure S10: ^{13}C NMR spectra of 3 (100 MHz). Figure S11: ^{1}H NMR spectra of 10 (400 MHz). Figure S12: ^{13}C NMR spectra of 10 (100 MHz). Figure S13: ^{1}H NMR spectra of 12 (400 MHz). Figure S14: ^{13}C NMR spectra of 12 (100 MHz). Figure S15: ^{1}H NMR spectra of 14 (400 MHz). Figure S16: ^{13}C NMR spectra of 14 (100 MHz). Figure S17: ^{1}H NMR spectra of 4 (400 MHz). Figure S18: ^{13}C NMR spectra of 4 (100 MHz). Figure S19: ^{1}H NMR spectra of 5 (400 MHz). Figure S20: ^{13}C NMR spectra of 5 (100 MHz). Figure S21: ^{1}H NMR spectra of B-Ph (400 MHz). Figure S22: ^{13}C NMR spectra of B-Ph (100 MHz). Figure S23: ^{1}H NMR spectra of B-Car (400 MHz). Figure S24: ^{13}C NMR spectra of B-Car (100 MHz). Figure S25: ^{1}H NMR spectra of B-Pheno (400 MHz). Figure S26: ^{13}C NMR spectra of B-Pheno (100 MHz). Figure S27: ^{1}H NMR spectra of B-ref (400 MHz). Figure S28: ^{13}C NMR spectra of B-ref (100 MHz).

Author Contributions: Synthesis of materials, X.-F.S. and M.W.; methodology, X.-F.S. and M.W.; analysis, X.-F.S., M.W., and J.T.S.; manuscript preparation, X.-F.S., M.W., A.T., and T.I. All authors have read and agreed to the published version of the manuscript.

Funding: This study was supported by the Grant-in-Aids for Science Research (17H04888 and 15K05432) from the Ministry of Education, Culture, Sports, Science, and Technology (MEXT, Japan), the Strategic International Collaborative Research Program (SICORP) concerning "Research on Hydrogen as a renewable energy carrier" from the Japan Science and Technology Agency (JST), and the Iwatani Naoji Foundation. M.W. acknowledges the support from I2CNER, funded by the World Premier International Research Center Initiative (WPI), MEXT, Japan.

Acknowledgments: The computation was carried out by using the computer resources offered under the category of General Projects by the Research Institute for Information Technology, Kyushu University.

Conflicts of Interest: The authors declare no conflict of interest.

References

1. Staffell, I.; Scamman, D.; Abad, A.V.; Balcombe, P.; Dodds, P.E.; Ekins, P.; Shah, N.; Ward, K.R. The role of hydrogen and fuel cells in the global energy system. *Energy Environ. Sci.* **2019**, *12*, 463–491. [CrossRef]
2. Staykov, A.; Lyth, S.M.; Watanabe, M. Photocatalytic Water Splitting. In *Hydrogen Energy Engineering. A Japanese Perspective*; Sasaki, K., Li, H.-W., Hayashi, A., Yamabe, J., Ogura, T., Lyth, S.M., Eds.; Springer: Minato city, Tokyo, Japan, 2016; pp. 159–174.
3. Barber, J. Hydrogen derived from water as a sustainable solar fuel: Learning from biology. *Sustain. Energy Fuels* **2018**, *2*, 927–935. [CrossRef]
4. Takata, T.; Domen, K. Particulate Photocatalysts for Water Splitting: Recent Advances and Future Prospects. *ACS Energy Lett.* **2019**, *4*, 542–549. [CrossRef]

5. Chen, S.; Takata, T.; Domen, K. Particulate photocatalysts for overall water splitting. *Nat. Rev.* **2017**, *2*, 17050. [CrossRef]
6. Ashford, D.L.; Gish, M.K.; Vannucci, A.K.; Brennaman, M.K.; Templeton, J.L.; Papanikolas, J.M.; Meyer, T.J. Molecular Chromophore—Catalyst Assemblies for Solar Fuel Applications. *Chem. Rev.* **2015**, *115*, 13006–13049. [CrossRef]
7. Wang, Q.; Domen, K. Particulate Photocatalysts for Light-Driven Water Splitting: Mechanisms, Challenges, and Design Strategies. *Chem. Rev.* **2020**, *120*, 919–985. [CrossRef]
8. Watanabe, M. Dye-sensitized photocatalyst for effective water splitting catalyst. *Sci. Tech. Adv. Mater.* **2017**, *18*, 705–723. [CrossRef]
9. Zhang, X.; Peng, T.; Song, S. Recent advances in dye-sensitized semiconductor systems for photocatalytic hydrogen production. *J. Mater. Chem. A* **2016**, *4*, 2365–2402. [CrossRef]
10. Loudet, A.; Burgess, K. BODIPY Dyes and Their Derivatives: Syntheses and Spectroscopic Properties. *Chem. Rev.* **2007**, *107*, 4891–4932. [CrossRef]
11. Boens, N.; Verbelen Ortiz, M.J.; Jiao, L.; Dehaen, W. An unexpected coupling–reduction tandem reaction for the synthesis of alkenyl-substituted BODIPYs. *Coord. Chem. Rev.* **2019**, *399*, 213024. [CrossRef]
12. Shimizu, S. aza-BODIPY synthesis towards vis/NIR functional chromophores based on a Schiff base forming reaction protocol using lactams and heteroaromatic amines. *Chem. Commun.* **2019**, *55*, 8722–8743. [CrossRef] [PubMed]
13. Ho, D.; Ozdemir, R.; Kim, H.; Earmme, T.; Usta, H.; Kim, C. BODIPY-Based Semiconducting Materials for Organic Bulk Heterojunction Photovoltaics and Thin-Film Transistors. *ChemPlusChem* **2019**, *84*, 18–37. [CrossRef] [PubMed]
14. Kowada, T.; Maeda, H.; Kikuchi, K. BODIPY-based probes for the fluorescence imaging of biomolecules in living cells. *Chem. Soc. Rev.* **2015**, *44*, 4953–4972. [CrossRef] [PubMed]
15. Farràs, P.; Cucinotta, F. Recent advances in artificial photosynthetic systems at Newcastle University. *C.R. Chimie* **2017**, *20*, 272–282. [CrossRef]
16. Zheng, B.; Sabatini, R.P.; Fu, W.-F.; Eum, M.-S.; Brennessel, W.W.; Wang, L.; McCamant, D.W.; Eisenberg, R. Light-driven generation of hydrogen: New chromophore dyads for increased activity based on Bodipy dye and Pt(diimine)(dithiolate) complexes. *PNAS* **2015**, *112*, E3987–E3996. [CrossRef] [PubMed]
17. Wang, P.; Guo, S.; Wang, H.-J.; Chen, K.-K.; Zhang, N.; Zhang, Z.-M.; Lu, T.-B. A broadband and strong visible-light-absorbing photosensitizer boosts hydrogen evolution. *Nat. Commun.* **2019**, *10*, 3155. [CrossRef]
18. Yang, H.; Wang, J.; Ma, J.; Yang, H.; Zhang, J.; Lv, K.; Wen, L.; Peng, T. A novel BODIPY-based MOF photocatalyst for efficient visible-light-driven hydrogen evolution. *J. Mater. Chem. A* **2019**, *7*, 10439–10445. [CrossRef]
19. Yang, H.; Zhao, M.; Zhang, J.; Ma, J.; Wu, P.; Liu, W.; Wen, L. A noble-metal-free photocatalyst system obtained using BODIPY-based MOFs for highly efficient visible-light-driven H_2 evolution. *J. Mater. Chem. A* **2019**, *7*, 20742–20749. [CrossRef]
20. Ye, C.; Wang, X.-Z.; Li, J.-X.; Li, Z.-J.; Li, X.-B.; Zhang, L.-P.; Chen, B.; Tung, C.-H.; Wu, L.-Z. Protonated Graphitic Carbon Nitride with Surface Attached Molecule as Hole Relay for Efficient Photocatalytic O_2 Evolution. *ACS Catal.* **2016**, *6*, 8336–8341. [CrossRef]
21. Yadav, R.-K.; Baeg, J.-O.; Kumar, A.; Kong, K.; Oh, G.H.; Park, N.-J. Graphene—BODIPY as a photocatalyst in the photocatalytic—Biocatalytic coupled system for solar fuel production from CO_2. *J. Mater. Chem. A* **2014**, *2*, 5068–5076. [CrossRef]
22. Huang, L.; Zhao, J.; Guo, S.; Zhang, C.; Ma, J. Bodipy Derivatives as Organic Triplet Photosensitizers for Aerobic Photoorganocatalytic Oxidative Coupling of Amines and Photooxidation of Dihydroxylnaphthalenes. *J. Org. Chem.* **2013**, *78*, 5627–5637. [CrossRef] [PubMed]
23. Wang, H.; Wagner, G.W.; Lu, A.X.; Nguyen, D.L.; Buchanan, J.H.; McNutt, P.M.; Karwacki, C.J. Photocatalytic Oxidation of Sulfur Mustard and Its Simulant on BODIPY-Incorporated Polymer Coatings and Fabrics. *ACS Appl. Mater. Interfaces* **2018**, *10*, 18771–18777. [CrossRef] [PubMed]
24. Zhou, Y.; Zhou, Z.; Li, Y.; Yang, W. Synthesis and properties of BODIPY polymers and their photocatalytic performance for aerobic oxidation of benzylamine. *Catal. Commun.* **2015**, *64*, 96–100. [CrossRef]
25. Liras, M.; Pintado-Sierra, M.; Iglesias, M.; Sánchez, F. A deprotection strategy of a BODIPY conjugated porous polymer to obtain a heterogeneous (dipyrrin)(bipyridine)ruthenium (II) visible light Photocatalyst. *J. Mater. Chem. A* **2016**, *4*, 17274–17278. [CrossRef]

26. Tachikawa, T.; Yamashita, S.; Majima, T. Evidence for Crystal-Face-Dependent TiO_2 Photocatalysis from Single-Molecule Imaging and Kinetic Analysis. *J. Am. Chem. Soc.* **2011**, *133*, 7197–7204. [CrossRef] [PubMed]
27. Wang, D.-G.; Tan, P.; Wang, H.; Song, M.; Pan, J.; Kuang, G.-C. BODIPY modified *g*-C_3N_4 as a highly efficient photocatalyst for degradation of Rhodamine B under visible light irradiation. *J. Solid State Chem.* **2018**, *267*, 22–27. [CrossRef]
28. Suryani, O.; Higashino, Y.; Sato, H.; Kubo, Y. Visible-to-Near-Infrared Light-Driven Photocatalytic Hydrogen Production Using Dibenzo-BODIPY and Phenothiazine Conjugate as Organic Photosensitizer. *ACS Appl. Energy Mater.* **2019**, *2*, 448–458.
29. Erten-Ela, S.; Yilmaz, M.; Icli, D.; Dede, Y.; Icli, S.; Akkaya, E.U. A Panchromatic Boradiazaindacene (BODIPY) Sensitizer for Dye-Sensitized Solar Cells. *Org. Lett.* **2008**, *10*, 3299–3302. [CrossRef]
30. Qin, C.; Mirloup, A.; Leclerc, N.; Islam, A.; El-Shafei, A.; Han, L.; Ziessel, R. Molecular Engineering of New Thienyl-Bodipy Dyes for Highly Effi cient Panchromatic Sensitized Solar Cells. *Adv. Energy Mater.* **2014**, *4*, 1400085. [CrossRef]
31. Watanabe, M.; Sun, S.; Ishihara, T.; Kamimura, T.; Nishimura, M.; Tani, F. Visible Light-Driven Dye-Sensitized Photocatalytic Hydrogen Production by Porphyrin and its Cyclic Dimer and Trimer: Effect of Multi-Pyridyl-Anchoring Groups on Photocatalytic Activity and Stability. *ACS Appl. Energy Mater.* **2018**, *1*, 6072–6081. [CrossRef]
32. Zhang, L.; Cole, J.M. Anchoring Groups for Dye-Sensitized Solar Cells. *ACS Appl. Mater. Interfaces* **2015**, *7*, 3427–3455. [CrossRef] [PubMed]
33. Parry, E.P. An infrared study of pyridine adsorbed on acidic solids. Characterization of surface acidity. *J. Catal.* **1963**, *2*, 371–379. [CrossRef]
34. Watanabe, M.; Hagiwara, H.; Ogata, Y.; Staykov, A.; Bishop, S.R.; Perry, N.H.; Chang, Y.J.; Ida, S.; Tanaka, K.; Ishihara, T. Impact of alkoxy chain length on carbazole-based, visible light-driven, dye sensitized photocatalytic hydrogen production. *J. Mater. Chem. A* **2015**, *3*, 21713–21721. [CrossRef]
35. Yang, W.; Prabhakar, R.R.; Tan, J.; Tilley, S.D.; Moon, J. Strategies for enhancing the photocurrent, photovoltage, and stability of photoelectrodes for photoelectrochemical water splitting. *Chem. Soc. Rev.* **2019**, *48*, 4979–5015. [CrossRef] [PubMed]
36. Hongxing, D.; Qiuoing, L.; Yuehui, H. Preparation of nanoporous $BiVO_4/TiO_2$/Ti film through electrodeposition for photoelectrochemical water splitting. *R. Soc. Open Sci.* **2018**, *5*, 180728. [CrossRef] [PubMed]
37. Pellegrin, Y.; Odobel, F. Sacrificial electron donor reagents for solar fuel production. *C.R. Chim.* **2017**, *20*, 283–295. [CrossRef]



© 2020 by the authors. Licensee MDPI, Basel, Switzerland. This article is an open access article distributed under the terms and conditions of the Creative Commons Attribution (CC BY) license (http://creativecommons.org/licenses/by/4.0/).